Physica Medica 46 (2018) 114–123

Contents lists available at ScienceDirect

Physica Medica

journal homepage: www.elsevier.com/locate/ejmp

Original paper

Task-based phantom evaluation of cardiac catheterization imaging modes

Lukmanda Evan Lubis[a,*], Leonard Airell Craig[a], Hilde Bosmans[b], Djarwani Soeharso Soejoko[a]

[a] Department of Physics, Faculty of Mathematics and Natural Sciences, Universitas Indonesia, Depok 16424, Indonesia
[b] Medical Imaging Research Center, Catholic University of Leuven, Leuven 3000, Belgium

ARTICLE INFO

Keywords:
Cardiac catheterization
Dose
Figure of merit
Image quality
Optimization

ABSTRACT

This study aimed to quantify the dose and quality of the preprogrammed imaging modes on two cardiac angiography devices (Philips Allura FD10 Clarity and Allura FD10) using a task-specific in-house phantom, and to discuss the appropriateness of the pre-programmed settings. A Figure of Merit (FOM), defined as the squared Signal Difference to Noise Ratio (SDNR) divided by Entrance Surface Air Kerma (ESAK), was calculated for phantom inserts with different sizes and concentrations of iodine, as well as tin foils. For the Allura FD10 Clarity device, the low dose fluoroscopic mode was found to be very dose efficient, while the available ciné modes should only be used for cases with high demand for contrast and temporal resolutions. For both devices, the basic beam spectrum of the low dose fluoroscopic mode should be explored for use on other imaging modes. Ciné modes for the Allura FD10 device differ only by their spatial resolution characteristics and have almost identical dose per frame. This study also found that tin may not be a suitable replacement for iodine for research purposes due to mismatching SDNR. The number of recommendations formulated for these two devices suggests that comparative dose and image quality tests of all routinely used imaging modes should be an obligatory part of the physicists' acceptance testing.

1. Introduction

Cardiac catheterization procedures are now a worldwide standard of practice for cardiac diseases [1,2]. The involvement of X-ray imaging for these complex procedures is potentially associated with deterministic effects such as skin damage, hair loss and severe necrosis above specific dose thresholds [3–8]. In addition, as with any other use of X-rays, there is a stochastic risk for neoplasm formation that increases with increasing exposure [4]. Dose monitoring is recommended for all patient groups, from children to obese patients and it is necessary to optimize the procedures. The required quality should be produced with a dose that is as low as reasonably achievable [4,9–11].

The patient's detriment from cardiac procedures is mainly governed by the tube current-exposure time product (mAs), tube voltage (kVp), filtration, patient attenuation, and the body part examined. Today, the exposure parameters are controlled automatically for both fluoroscopy and ciné acquisition modes by an Automatic Exposure Rate Control (AERC) unit. Understanding the settings of such units plays a key role in determining the optimal imaging modes for given groups of patients and allows subsequent proper in-room training and feedback. Following the European and International Basic Safety Standards [12,13], the medical physics expert should be involved in these tasks, but detailed procedures have not been introduced, and experience is therefore limited.

In present study, image quality was studied through the measurement of signal from a dedicated, newly developed contrast-detail test object. Detectability of the inserts is influenced by several components of the imaging chain, including beam quality and dose rate. The specific quantitative parameter employed was Signal Difference-to-Noise Ratio (SDNR), calculated from iodinated contrast agents provided in a blood vessel shaped insert. Radiation detriment was expressed in terms of entrance skin dose (ESD) [14,15]. The Entrance Surface Air Kerma (ESAK) is related to the ESD through the back-scatter factor, which does not vary greatly for cardiac procedures, and is utilized in this study. This Figure of Merit was first introduced by Zamenhof et al. [16]. Aim of the study was to investigate the AERC modes on two angiographic X-ray systems used for adult cardiac procedures with the dedicated phantom, and plan, if needed, further optimization or teaching actions.

2. Materials and methods

The study was performed on two Philips Allura FD10 devices (Philips Medical System, Best, the Netherlands), both in operation in the Invasive Cardiology Department, Pertamina Central Hospital, Jakarta. The first device was an Allura FD10 with a maximum flat detector size of 20 cm × 20 cm. The maximum nominal voltage applied to the MRC 200 0508 ROT-GS 1003 X-ray tube was 125 kVp with a maximum output of 1250 mA at 80 kV. The tube had a permanent filtration of 2.5 mm Al with additional filters of 0.1 mm Cu, 0.4 mm Cu, and 1.0 mm Al and two

* Corresponding author.
E-mail address: lukmanda.evan@sci.ui.ac.id (L.E. Lubis).

https://doi.org/10.1016/j.ejmp.2018.02.002
Received 12 October 2016; Received in revised form 19 December 2017; Accepted 1 February 2018
Available online 05 February 2018

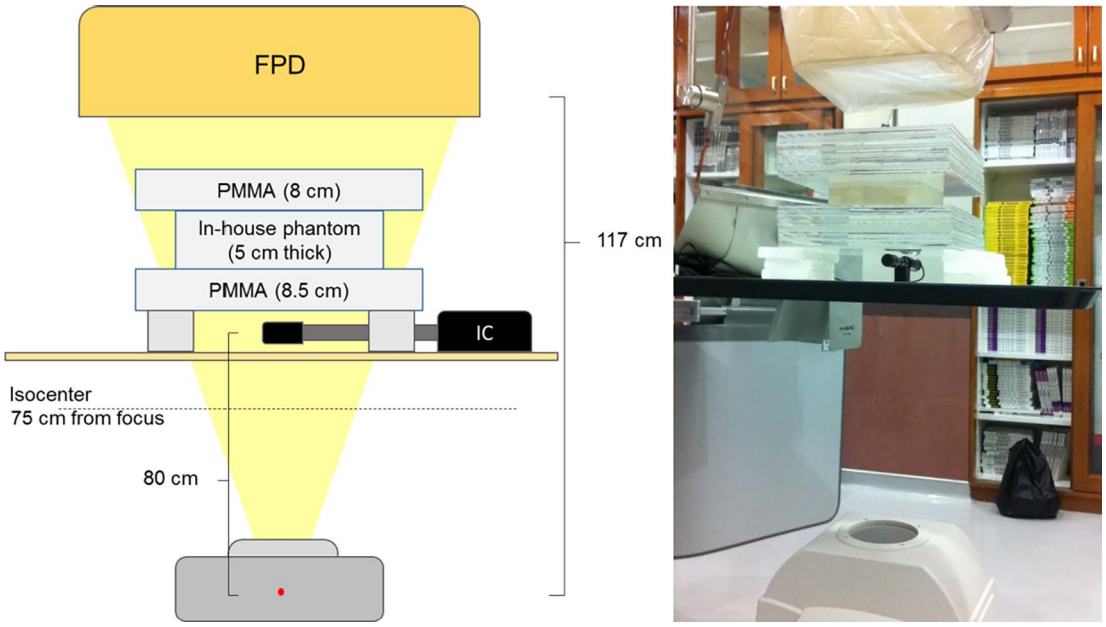

Fig. 1. Arrangement of X-ray tube, phantom and image flat-panel detectors (FPD) (left) (not to scale), and real arrangement (right). (IC = ionization chamber, PMMA = poly methyl methacrylate).

nominal focal spot sizes of 0.5 mm and 0.8 mm. The device was equipped with Clarity software for dose reduction and image quality enhancement [17–19]. The second device was an older Allura FD10 with identical technical details to the above but without the Clarity software in place. Prior to the study, performance testing of both devices had been performed by the X-ray Compliance Test Service Division of the Medical Physics and Biophysics Laboratory of Universitas Indonesia, using the technical test procedures of the Indonesian Nuclear Energy Regulatory Agency. Additional tests in compliance with AAPM Report No. 70 were also performed [20].

A 5 cm thick PMMA phantom was constructed in house (Fig. 1), and contains tubes with different internal diameters of 1 mm, 2 mm, 4 mm, 6 mm, and 8 mm. They were filled with 300 mg/cc iodine contrast agents that were diluted to blood plasma concentrations of 14%, 16%, 18%, and 20%. The concentrations were determined as in our previous work [9], and had been optimized to represent typical injections in adult patients. The samples were prepared at the Biophysics Laboratory, Universitas Indonesia. At the mid-plane of the phantom, we put tin foils of 99.98% purity, a thickness of 127 μm and sizes as the iodine tubes. Tin was selected for its similarity with iodine in terms of K-edge [21].

2.1. Experimental setup

The measurement geometry was set to represent the clinical PA projection (Fig. 1). The measured source-to-image distance (SID) was 117 cm, in accordance with typical clinical settings. For the same reasons, the anti-scatter grid was used during the entire work. The distance between the tube focus and dosimeter was 80 cm.

Stacks of PMMA slabs of each 0.5 cm thick and the in-house phantom were positioned in a sandwich-like manner to reach the posterior-anterior (PA) thickness of a typical Indonesian adult chest, which is 21.5 cm, based on a study by Manuaba [22]. A total of 8 cm and 8.5 cm PMMA slabs were placed on and below the phantom, respectively. An air gap of about 15 cm was kept between the top of the phantom and the detector to simulate space for anesthetic devices in clinical condition.

2.2. Imaging parameters

The exposures were made using both devices with the 'adult cardio' patient selection protocol using the AERC for fluoroscopic and ciné acquisition modes. There are three dose modes for each device in fluoroscopy, while in ciné a number of modes with various pulse-rates are selectable. Table 1 lists the exposure parameters for each mode for the 21.5 cm-thick object. Tube filtration was fixed for all pre-programmed modes. To accommodate the size of the in-house phantom, only the full FOV (25 cm) was used in the study. Magnification modes were not tested. The mean energy of the beam was calculated using the method described by Boone and Seibert (1997) [23], assuming a 3 mm of half-value layer for each beam.

2.3. Dose estimation and image quality analysis

A Radcal®10X6-6 with 6 cc of active volume ionization chamber (IC) was used to measure the ESAK at the surface of the phantom. Ionization chamber was positioned to include backscatter [24]. This dosimeter does not influence the settings of the AERC. The ESAK values from all exposure modes were recorded for subsequent calculation of the FOM.

The images of all exposure modes (at least three images for each imaging mode) were recorded in DICOM format and analysed using ImageJ software. Among the series of images produced per exposure, one frame was randomly selected for image quality assessment utilizing SDNR measurements. The SDNR is based on measurement of the mean pixel value and its standard deviation for rectangular regions of interest (ROIs) for each vessel diameter and tin foil, using corresponding areas of background. Typical positions of the ROIs are shown in Fig. 2. SDNR was calculated using Eq. (2), in which N_B is the mean pixel value of the background ROI, located adjacent to the simulated vessels and the tin foil, and SD_B is the standard deviation of the same ROI. The parameter N_O is the object mean pixel value of the ROI located inside the simulated vessel or in the tin foil and SD_O is the standard deviation of the same ROI [16,25–27].

$$SDNR = \frac{N_B - N_O}{\sqrt{\frac{(SD_O^2 + SD_B^2)}{2}}} \quad (1)$$

$$FOM = \frac{SDNR^2}{ESAK} \quad (2)$$

At least three repetitions were made for both image quality and dose measurements and average values were retrieved. Figure of Merit values were calculated for all measurements along with the standard deviations. The attributed error is addressed as the combined uncertainty utilizing the standard deviation of the repeated measurements performed for each condition and dose measurement instrument uncertainty (shown in Figs. 3–7 as solid error bars).